PNAS RESEARCH ARTICLE | EARTH, ATMOSPHERIC, AND PLANETARY SCIENCES OPEN ACCESS

Shelf-invading low-oxygen waters control Cenozoic organic carbon burial rates

Rosalind E. M. Rickaby[a,1], Thomas J. Wood[a], Zunli Lu[b], and Christian J. Bjerrum[c]

Affiliations are included on p. 8.

Edited by Eric Rignot, University of California Irvine, Irvine, CA; received September 26, 2025; accepted April 21, 2026

The thermostatic mechanisms of Earth's persistent habitability remain unresolved. High-resolution Cenozoic C isotope records, P accumulation, and coarse-fraction I/Ca allow recalculation and assessment of controls on the global proportion of total carbon buried as organic carbon (f_{org}), a regulator of atmospheric CO_2 and O_2. f_{org} was suppressed during the Eocene hothouse, coincident with an oxygenated water column and low water-column phosphate. With decreased sea level, the area for efficient organic carbon and phosphate sedimentary burial diminished, leading increasingly to greater water-column phosphate, higher primary productivity, and emergent water column deoxygenation. The sea-level influence on the areal extent of high sedimentation in shelf regions acts as a control on phosphate availability for new production, respiratory demand, and ocean oxygenation, as proposed by hypsographic models [C. J. Bjerrum, J. Bendtsen, J. J. F. Legarth, *Geochem. Geophys. Geosys.* 7, 1–24 (2006)]. During intermediate sea-level highs of the Neogene, pulses of enhanced organic carbon burial prevailed for multimillion years, in response to the redox recycling of phosphate when oxygen minimum zones with O_2 < 90 μmol/kg were present. We propose the existence of a self-limiting intermediate sea-level sweet spot with peak C_{org} burial due to redox recycling of phosphate, whereby oxygen minimum zones (OMZ) with O_2 < 90 μmol/kg impinge on the most C_{org} rich continental shelf sediments. Such a sweet spot has narrowed over Earth history due to deepening OMZs, stabilizing both atmospheric O_2 and CO_2. Continental marine inundation controls on phosphate availability, and the sedimentary carbon flux, provide a positive-feedback and rectifier to perturbations during inception of the icehouse world.

carbon cycle | sea level | oxygen minimum zone | phosphate | carbon isotopes

Significance

Unresolved mechanisms stabilize our planet's atmosphere. Cenozoic reconstructions of burial rates of organic carbon and phosphorus, and water column oxygenation reveal the first-order feedback between the degree of continental shelf flooding and ocean productivity. Limited aqueous P availability at high sea level, due to efficient continental shelf burial, starved the ocean sedimentary carbon sink, oxygenated the ocean, and led to atmospheric CO_2 accumulation. Lower sea levels harbored increasing P and emergent deoxygenated waters. The extent of interaction between ocean low-oxygen zones and shelf sediments defines a sea-level "sweet-spot" for rapid burial of organic carbon which acts as a rectifier of glacial conditions. The geological deepening of oxygen minimum zones (OMZs) increasingly stabilized CO_2 and O_2 in Earth's atmosphere.

Atmospheric Composition Thermostats. Interacting redox feedbacks have rarely been considered as key drivers of atmosphere and ocean chemistry over the Cenozoic. A temperature-dependent silicate weathering feedback (1) is thought to keep the sources of CO_2 from the outgassing of volcanoes, and from organic matter weathering, in balance with the sedimentary sinks of $CaCO_3$ and organic carbon. Similarly, a thermostat may regulate atmospheric O_2 since any increase in oxidative weathering drives an increase in the burial rate of C_{org}, catalyzed by the redox recycling of P, which self-rectifies due to oxygenation over multimillion year timescales (2). The burial rate of organic carbon acts as a link between these two thermostats and their control on atmospheric CO_2 and O_2 by acting as a sink of carbon, and a source of oxygen to the atmosphere on long timescales (3), as well as acting as a fast feedback capable of driving instability in the climate system (4).

On long timescales, the amount of organic carbon produced in the ocean is assumed to be limited by the availability of aqueous phosphorus (P_{aq}), supplied by continental weathering (5). Phosphorus is an irreplaceable nutrient utilized by all organisms (6). The intimate linkage between C and P during burial limits extended periods of C_{org} burial in the past due to the efficient removal of P from the water column (7). P_{aq} is buried in three main forms: organic-, iron-, and calcium-associated P, collectively referred to as P_{reac}. Under anoxic bottom waters, the burial of organic and/or iron associated P is suppressed, resulting in C_{org}/P_{reac} increasing from ~50 in bioturbated muds under oxic conditions to ~250 in laminated muds under anoxic conditions (8–12) Also, bulk sedimentation rate and the C_{org}/P_{reac} have a nonlinear relationship with the highest C_{org}:P_{reac} ratios at intermediate sedimentation rates (13–15). Under anoxic conditions, the reduction of iron oxy-hydroxides to ferrous iron in solution releases phosphate (10). Consequently, phosphate recycling to the water column is greater from carbon-rich sediments overlain by

Author contributions: R.E.M.R. designed research; R.E.M.R. and Z.L. performed research; R.E.M.R., T.J.W., Z.L., and C.J.B. analyzed data; and R.E.M.R., T.J.W., Z.L., and C.J.B. wrote the paper.

The authors declare no competing interest.

This article is a PNAS Direct Submission.

[1]To whom correspondence may be addressed. Email: rosr@earth.ox.ac.uk.

This article contains supporting information online at https://www.pnas.org/lookup/suppl/doi:10.1073/pnas.2526409123/-/DCSupplemental.

Published June 22, 2026.

oxygen-depleted waters at intermediate sedimentation rates on the outer shelf and upper slope (8, 10, 13, 16, 17).

The importance of the degree of inundation of the shelf as an amplifying-feedback on climate has been considered in terms of the enhanced alkalinity of a lower sea-level ocean coined the "coral reef hypothesis" (18, 19) and the impact of decreased sea level on carbon and phosphate burial on shelves during glacials (20). At low sea level, more nutrients have been proposed to have been transferred to the deep ocean, resulting in higher P_{aq} and less dissolved oxygen (Fig. 1). Bjerrum et al. (7) used hypsographic modeling to show that a sea level decrease of order of 200 m is sufficient to change the residence time of phosphate from ~10 ky to ~50 ky and to more than double the average P_{aq} concentration due to the decreased area available for efficient C_{org} and P_{org} burial in the shallowest sediments (Fig. 1 *A*, *B*, and *D*). Such a sea-level dependence of P_{aq} availability on C_{org} and P_{org} burial is increasingly invoked to account for a significant fraction of the CO_2 oscillation during glacial-interglacial cycles (21–23).

Here, we demonstrate that the hypsographic models of seawater compositional change due to sea level, and the intimate coupling between the oxygen, phosphorus, and carbon cycles is supported by data through the Cenozoic Era. The sedimentary burial rate of carbon as both carbonate and organic carbon was significantly reduced during the Eocene hothouse (56 to 33.9 Ma), coincident with the period of highest atmospheric CO_2 and suggestive that an imbalance between weathering source and sedimentary sink led to an accumulation of carbon in the atmosphere. At this time, the ocean was highly oxygenated, as evidenced from I/Ca. Coincidently, low P in pelagic deep-sea sediments indicated an extended period of phosphate starvation which inhibited primary production, reduced the sedimentary sink of carbon, and plausibly drove an imbalance in the carbon cycle of the Eocene hothouse world.

Results

Reconstruction of Fractional Burial Rates of Organic Carbon. The size of the sedimentary organic carbon reservoir over time plays a fundamental role in the long-term oxidation of the Earth's surface environment (24). Due to the ~25‰ C isotopic fractionation associated with fixation of carbon via Rubisco (25, 26), the carbon isotopic composition of the ocean provides a uniquely global measure of the proportional rates of C_{org} burial relative to the $CaCO_3$ sink, assuming the isotopic composition of the carbon input remains quasi-constant (27). The isotopic composition of the carbon input may change (*SI Appendix*, *SI Text*) due to kerogen weathering (28) or to variance in the solid Earth degassing signature (29). The near consistency of the average ocean C isotopic composition at +2‰ throughout a billion years of geological history suggests that the input has remained largely constant at ~–6‰ (30) despite significant perturbations in tectonism, exposure of older sediments and the terrestrial biota.

Mass balances of C fluxes are often calculated assuming that organic matter is buried with a $\delta^{13}C$ ~ –25‰ lighter than the ocean. This fractionation factor is measured in the Rubisco enzyme isolated from spinach and is not representative of algal Rubisco fractionation, which may have evolved to be as small as ~ -11‰ (31). To circumvent uncertainties in the magnitude of the fractionation associated with the diversity of affinity of Rubisco for CO_2 fixation, it is possible to compile a record of the $\delta^{13}C$ of marine C_{org} which implicitly accounts for a variable fractionation factor, rather than relying on the assumption of a fractionation factor. A new compilation, used for the reconstruction of pCO_2 (32), also provides the most complete and continuous dataset of

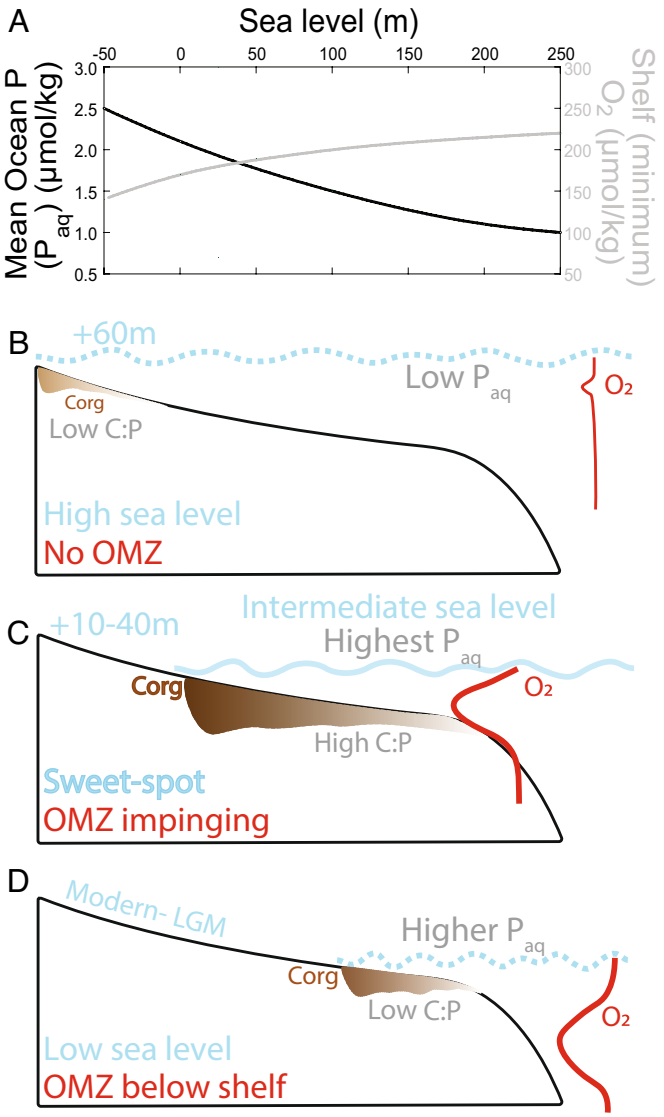

Fig. 1. The relationship between sea level, P_{aq} (black), and water column minimum O_2 (gray) as found by hypsographic modeling plotted as solid curves (*A*), redrawn from steady state model results of Bjerrum et al. (figure 6C from ref. 7). Panels (*B–D*): C_{org} burial rates are indicated by the brown shading with annotations to indicate the C_{org}/P_{reac} of that burial, with low C_{org}/P_{reac} at the high and low sedimentation rates of the coastal and pelagic realms, but high C_{org}/P_{reac} at intermediate sedimentation rates (12, 14, 15). P_{reac} is most efficiently buried at the highest sea levels (>+50 m) with the greatest area of shallow coastal sediments, yielding the lowest P_{aq}, which restricts organic carbon production globally (*A*). At sea-levels <+50 m, P_{aq} is more available for the production of C_{org}, which increases the respiratory burden of the water column, leading to the emergence of an oxygen minimum zone. At water column O_2 concentrations <90 µmol/kg, P_{aq} release from sediments is triggered which allows extensive C_{org} burial. This is most effective when those minimum O_2 waters still impinge on the C_{org}-rich sediments of the continental shelf at intermediate sea levels of +10 to +40 m (*C*). At lower sea levels still (<+10 m), the OMZs drop beneath the continental shelf and lie in contact with much lower C_{org} content sediments, restricting P_{reac} release, as is the case in the modern ocean (*D*). Further, the flux of P_{aq} from weathering may be limited due to the cold conditions in the glaciated world.

alkenone $\delta^{13}C$ (Fig. 2), a molecule exclusively produced by distinct species of coccolithophore. Alkenone $\delta^{13}C$ has been shown to be consistently offset by 4.2‰ from the isotopic composition of the bulk cellular biomass (33; *SI Appendix*, *SI Text*) and provides a measure of the $\delta^{13}C$ of marine sedimentary C_{org} without contamination from terrestrial sources.

Since approximately 30 Ma, the carbon isotope fractionation between alkenone $\delta^{13}C$ ($\delta^{13}C_{alk}$) and oceanic DIC has decreased

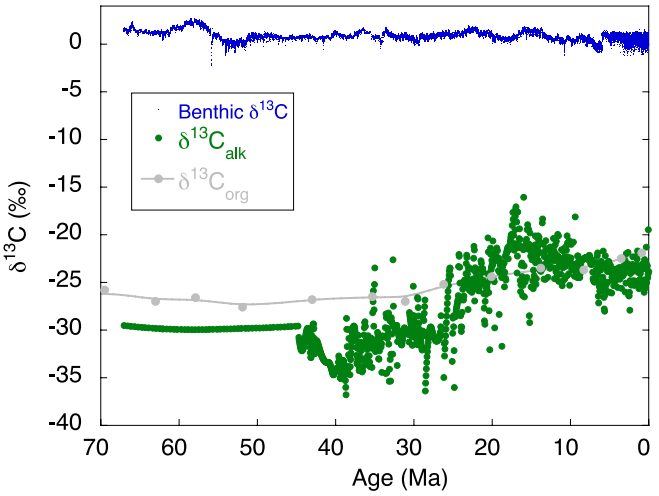

Fig. 2. Compiled records of carbon isotopes: benthic foraminifera, blue, (34); alkenones, green, corrected for the 4.2 ‰ offset from biomass (33, *SI Appendix*, *SI Text*) including interpolated low-resolution phytane (35) for the oldest parts of this record. A longer-term compilation of $\delta^{13}C$ of C_{org}, gray, from ref. 27 is plotted as interpolated data to obtain a common timescale.

from ~24 to ~16‰, from extrapolation of pre- and post-30 Ma data to a zero intercept (*SI Appendix*, Fig. S1). Such a trend toward a heavier isotopic composition of marine C_{org} toward the modern is also captured at lower resolution by Hayes et al. (27, Fig. 2). Insight into size-dependent intracellular reservoirs of carbon (36) suggests that the alkenone-producing coccolithophores have adapted on geological timescales to diminishing carbon availability by diminishing in size (37, 38), with a trade-off to faster division rate. This size adaptation also shrinks the internal cellular carbon pool but keeps it full, which allows a relaxation in the affinity of their Rubisco enzyme (39) with a concomitant reduction in enzymatic C isotopic fractionation (26, 40). As a result, the alkenone record, which is not species-specific, likely reflects the assemblage shift toward smaller, faster-growing species with a relaxed Rubisco affinity for carbon and a diminished Rubisco fractionation factor. That the change in fractionation factor is ~10‰ could reflect a switch in carbon substrate used from CO_2 to HCO_3^-.

The fractional burial flux of organic carbon C_{org} relative to total carbon (f_{org}) added to marine sediments for a given interval is

$$f_{org} = \left[\frac{\delta_{in} - \delta_{carb}}{\delta_{org} - \delta_{carb}}\right],$$

where δ_{carb} is $\delta^{13}C$ of carbonate deposition, δ_{org} is the $\delta^{13}C$ of C_{org} deposition, and δ_{in} is the mean isotopic composition of inputs to the ocean. Although Kump and Arthur (41) suggest the use of the shallow record of carbonate $\delta^{13}C$ for mass balance calculation, these records tend to suffer from bias and vital effects (42, 43). The high-resolution benthic $\delta^{13}C$ splice of Westerhold et al. (34) is used as a measure of the $\delta^{13}C_{carb}$ with a bulk carbonate to benthic offset of 0.9‰ (28).

The records of $\delta^{13}C_{org}$ and $\delta^{13}C_{carb}$ were interpolated at ~50 ky intervals to provide datasets at comparable resolution and age before calculation of f_{org}. Linear regression between the fractionation and $\delta^{13}C_{carb}$ (27) suggests that δ_{in} is poorly constrained by the data but approximates −6‰ in accord with Hayes et al. (27, *SI Appendix*, *SI Text*), and is close to the canonical value of volcanic degassing inputs (29). We recognize that δ_{in} variation may have some significance through the Cenozoic, but find its variation through time unconstrained with the current unknowns. For simplicity, we treat δ_{in} as a constant (*SI Appendix*, Fig. S2).

The f_{org} record shows a number of peaks and troughs with a multimillion-year wavelength varying in amplitude around a mean value of about a third of the carbon sink buried as organic carbon (Fig. 3). The main peaks in f_{org} are associated with sea-level highs, but not all sea-level highs are associated with peaks of relative organic carbon burial. Most notably, the f_{org} peak amplitude relative to sea-level prior to 23 Ma is more muted than during the sea-level highs in the later Oligo-Miocene (23 to 5.3 Ma). The individual peaks in f_{org} are supported by additional sedimentary evidence. The peak centered around 6 Ma coincides with the "biogenic bloom" (44–46), and that around 15 Ma with the Monterey event associated with large-scale economic hydrocarbon reservoirs (47, 48). The Paleocene–Eocene is known as a time of enhanced C_{org} burial (49, 50) and high inferred productivity. High C_{org} burial characterized the Oligo-Miocene as documented to harbor 12.5% of the world's oil reservoirs (~23 Ma) (51, 52). The rise in pO_2 associated with pulses of f_{org}, is coincident with, and could have permitted, significant nonallometric shifts in brain-body size of mammals and birds in the aftermath of the K/Pg extinction during the Paleocene and early Neogene (~23 Ma) (53, 54).

The Eocene suppression in f_{org} from the average of 0.3 down to ~0.2, for an extended period from ~50 to 30 Ma, is also supported by the identification of "missing C_{org}" in Eocene marine sediments, where C_{org} burial was depressed by an order of magnitude compared to modern (57). Overall, our record suggests that an increase in f_{org} is generally associated with sea-level rise during the Cenozoic, except for the extended period from ~50 to ~30 Ma when the proportional burial rates are suppressed significantly. This period is characterized, in part, by some of the highest sea levels of the last ~65 My at over 60 m above current sea levels during the Early Eocene.

Our reconstructed changes in f_{org}, calculated using a methodology sensitive to global burial rates, challenge earlier estimates based on sedimentary budgets (23, 58). In todays' oceans, the burial rate of C_{org} is highly laterally heterogeneous with up to 70% of burial constrained to narrow but areally extensive, high-sedimentation continental shelf regions (7, 14). Sedimentary budgets are susceptible to regional bias and suffer from challenges in the accuracy of accumulation rates that are necessarily derived from sediment thickness between two age points, each of which contains uncertainty.

Sea-Level Mediated Phosphate and Organic Carbon Burial. A first-order driver of the f_{org} record is the sea-level dependence on the availability of P_{aq} (7, 59). The lowest pelagic biogenic P accumulation rates [from Follmi (56)], a proxy for global P_{aq}, occurred between 45 Ma and 32 Ma, approximately coinciding with the period of lowest f_{org} (Fig. 3). Higher sea levels resulted in a reduced global ocean P_{aq} due to efficient C_{org} and P_{reac} burial on the associated wider continental shelf. In contrast, lower sea levels resulted in elevated P_{aq} due to burial with a higher C_{org}/P_{reac} on the minimal continental shelf and upper slope. P_{aq}-limitation of global productivity associated with high sea level therefore may account for the first-order observation of depressed proportional C_{org} productivity and burial during the highest sea levels of the Eocene (56 to 33.9 Ma) relative to the rest of the Cenozoic, a scenario that persisted for many millions of years.

That low pelagic biogenic P accumulation approximates P_{aq} is well supported by an association between low pelagic biogenic P accumulation and other indicators of oligotrophy. The increasing oligotrophy of the calcifying taxa through the Eocene (60) and a predominance of large heavily calcified forms [e.g., Claxton et al. (43)], characterized by low growth rates, are suggestive of adaptation to low nutrients and high CO_2 conditions. The pelagic biogenic P accumulation rates also suggest an extended period of

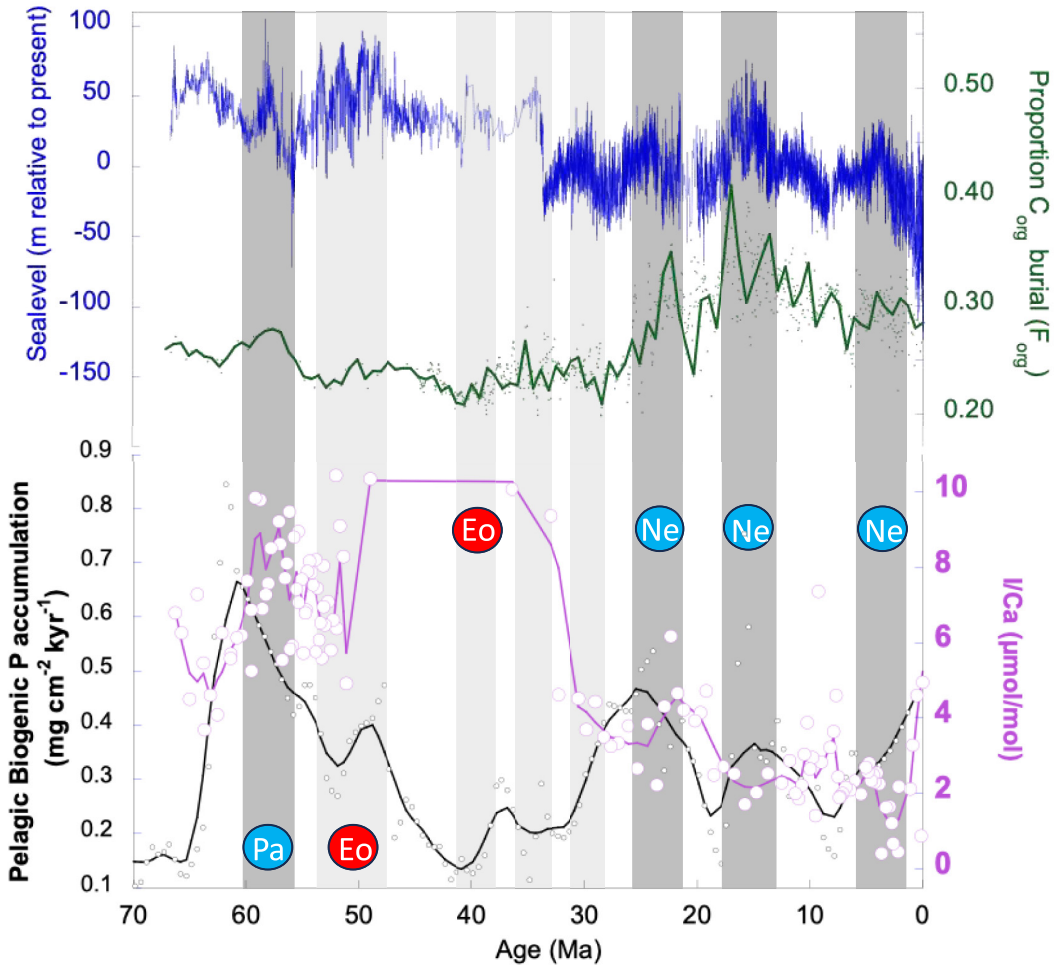

Fig. 3. Records of sea level (55), blue; reconstructed proportional burial flux of C_{org} based on the alkenone $\delta^{13}C$ record showing small green individual datapoints and an interpolated curve; an interpolated record of I/Ca of the coarse-fraction from site 1264 spliced with 1262 in the South Atlantic (open purple circles) (this study) and pelagic biogenic P accumulation in sediments with <5 wt% Al_2O_3, a proxy for P_{aq} (black, 56). The dark gray bars highlight the periods of time with higher proportional C_{org} burial, higher sea levels, higher pelagic biogenic P accumulation, and lower water column oxygen concentration. The light gray bars highlight the periods of higher sea-level fluctuations unmatched by C_{org} burial. During this period, pelagic biogenic P accumulation is low and water-column I/Ca is high. The red and blue circles denote the events (Paleocene Pa, Eocene Eo, and Neogene, Ne), which are then plotted in Fig. 5. The age model is from Westerhold et al. (34).

P_{aq} limitation during the late Cretaceous (100 to 66 Ma). The Late Cretaceous was also dominated by phytoplankton adapted to oligotrophic conditions when sea level was thought to still be ~100 m above present (61, 62).

Collectively, there are indications of higher f_{org} at intermediate sea levels (+0 to +40 m) (Fig. 4). The maintenance of a higher-than-average f_{org} for an extended multimillion-year timescale is challenging due to the short residence time of P_{aq} in the ocean (15 to 100 ky) (16). In order to explain the apparently extended pulses of f_{org} over 3 to 5 My accompanying sea-level highs outside of the Eocene high-stand, it is necessary to appeal to mechanisms that allowed replenishment of phosphate into the water column. This P sustained prolonged multimillion-year periods of C_{org} burial, via a redox sensitive recycling of phosphorus and elevated C_{org}/P_{reac} burial ratio (7–9, 16, 17, 63), which also led to more organic carbon burial per unit P delivered to the ocean.

Oxygen Minimum Zones (OMZ) Presence, P Availability, and Sea Level. It is possible to test this mechanism of redox-sensitive recycling of P as a driver of extended C_{org} burial using planktic foraminiferal I/Ca, a proxy for past water column O_2 concentrations (61). The principle of the proxy is that the speciation of iodine between the I^- ion and the IO_3^- ion is sensitive to O_2 availability, such that the reduction of IO_3^- to I^- is often observed in OMZs. It is only the IO_3^- ion that substitutes for the CO_3^{2-} and is incorporated into calcium carbonate fossils such as planktic foraminifera. Higher I/Ca ratios, in principle, indicate higher degrees of water column oxygenation. Existing core-top data show that planktic I/Ca < 2.3 µmol/mol in water columns represents O_2 beneath <90 µmol/kg (65–67); similar to the oxygen concentration threshold, related to anoxia in shallow porewaters, proposed for the release of P_{reac} back to the water column (7). Therefore, planktic I/Ca can serve as an independent constraint on the connection between P_{reac} accumulation rates and the reconstructed fractional C_{org} burial (Fig. 3).

We have measured the coarse-fraction (mixed species planktic foraminifera) I/Ca over the Cenozoic from Southern Atlantic Ocean (ODP Site 1262 and 1264). I/Ca is highest during the period of 30 to 50 Ma with values of ~8 to 10 µmol/mol, and trends to lower values from 30 Ma toward the modern day, with additional fluctuations above the ~2 µmol/mol background to values of ~4 µmol/mol at ~20 Ma, 10 Ma, and in the last 2 to 3 My. The high I/Ca in the Eocene (56 to 33.9 Ma), suggest that the O_2 content of the upper water column from 30 to 48 Ma could have exceeded 140 µmol/kg, based on a core-top study (64), qualitatively indicating that OMZs were absent from these sites during the

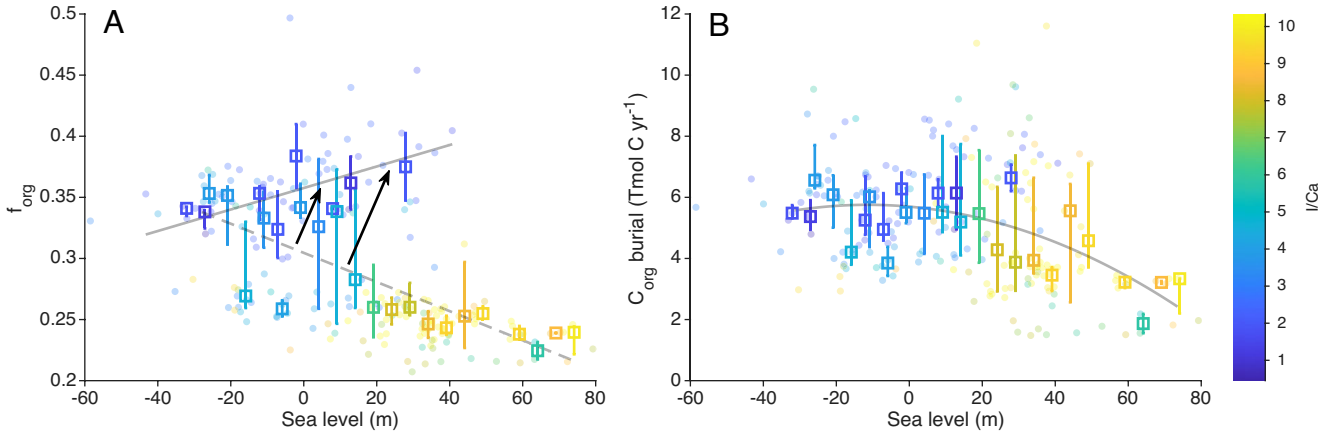

Fig. 4. Organic carbon cycle response to changes in Eustatic sea level. (*A*) Scatter of proportional C_{org} burial (f_{org}) against sea level (55), colored by the I/Ca ratio. f_{org} data were split above and below the I/Ca = 2.3 OMZ threshold of ref. 64, binned at 5 m sea-level intervals, and plotted as box (median) and whiskers (IQR) for bins with n > 2 datapoints, which were colored by I/Ca. Linear trendlines were drawn for f_{org} data at low I/Ca ≤ 2.3 (solid, r = 0.557, *P* = 2.5e-03) and at high I/Ca > 2.3 (dashed, r = −0.543, *P* = 2.7e-14). Black arrows show the approximate direction of sea-level associated perturbations from 23 Ma on in Fig. 3. (*B*) Scatter of calculated C_{org} burial flux against sea level, colored by I/Ca, a proxy for ocean oxygen levels, and overlain with boxes and whiskers as in (*A*). C_{org} burial flux data were overlain with a best-fit second-order polynomial, plotted between min and max sea level boxes. Note how organic burial tends toward an optimum between 0 and +40 m.

Eocene (Fig. 3). The decline in I/Ca to reach 2.3 µmol/mol sporadically suggests that OMZs with water column O_2 < 90 µmol/kg started to emerge and intensify at lower sea levels from the Oligocene onward.

Taking I/Ca as a measure of the oxygenation of the water column, during the Eocene, the water column oxygen content was elevated above the critical threshold of 90 µmol/kg. At such high water-column O_2 concentrations, phosphate is adsorbed onto iron oxyhydroxides which, along with C_{org} burial, results in a low C_{org}/P_{reac} burial ratio with phosphate efficiently buried in coastal sediments. Due to the highest sea levels from 33 to 48 Ma, at about +50 to +66 m above present-day sea level, C_{org} production, and water column O_2 consumption was limited by P_{aq} (7, Fig. 1). Consequently, the ocean harbored the lowest productivity and the water column became highly oxygenated in accord with the N isotopic signature during Cenozoic warm periods (68).

Since 30 Ma, water column deoxygenation emerged in response to declining sea levels below ~+40 m, as indicated by a decrease in I/Ca, and was driven toward a threshold of oceanic oxygen concentration < 90 µmol/kg. (Figs. 3 and 4*A*). These observations agree with model results in which lower sea levels resulted in reduction of the shelf area with high sedimentation rates for efficient C_{org} and P_{reac} burial. This resulted in an increase in P_{aq}, potentially amplified by an increase in P weathering input (69, 70) resulting in greater productivity of C_{org} and a greater respiratory burden for the water column (7) (Fig. 1*A*).

Increasing P_{aq} though the Neogene is further supported by the fossil record. Experiments indicate that coccolithophores grown at high P_{aq} decrease their calcification rate (71) because cell division becomes too fast for the diffusive carbon supply rate for calcification, such that calcite/cell decreases (72). Since the Eocene (56 to 33.9 Ma), coccolithophores have shrunk (37), with higher growth rates (73) and lower calcification intensities (43), suggestive of a community change in response to increasing P_{aq} and declining pCO_2. The fossil record of Cenozoic diatom size echoes this trend, so all plankton may respond in a similar way to elevated P_{aq} (74).

During the Neogene, increasing P_{aq} drove areas of the ocean close to but above the threshold O_2 content of ~90 µmol/kg (Figs. 4*A* and 5). Superimposed on the background trend, were perturbations. Each individual period of sea-level rise of up to +40 m above modern, was associated with an extended multimillion-year pulse of f_{org}, lower I/Ca ratios, and higher P availability (Figs. 3 and 4*A*). An incremental P input from an increase in weathering or from sea-level rise-associated coastal erosion was sufficient to push the ocean beneath the critical oxygen threshold (90 µmol/kg). Crossing this threshold triggered disproportionate phosphate release from sedimentary organic- and iron-associated P_{reac} (Fig. 1*C*) yielding carbon burial with a high C_{org}/P_{reac} and extended periods of high C_{org} burial (Fig. 4).

During the final stages of the Neogene, as sea level on average decreased below ~+10 m, f_{org} decreased, and the amplitude of perturbations diminished while I/Ca remained low (Figs. 3 and 4*A*). These observations suggest that once beneath the O_2 threshold (I/Ca ~ 2.3) for effective P regeneration, P_{aq} is high and small perturbations to the P inventory can no longer be amplified.

An Organic Carbon Burial Sweet Spot. Our Cenozoic data indicate that the relationship between eustatic sea level and f_{org} is nonlinear, with two trends separated by a threshold I/Ca of ~2.3 µmol/mol (64), with an instability and hysteresis in f_{org} at intermediate sea-levels (+0 to −40 m). Beneath this O_2 threshold, with I/Ca < 2.3 µmol/kg, f_{org} decreases with decreasing sea level (Fig. 4*A*). The two trends in f_{org} as a function of sea level, converge at a sea level of ~0 to −20 m, and tend toward lower f_{org} with further sea level decrease, associated with lower oxygen values, in agreement with high-resolution Pleistocene data (Fig. 4*A* and *SI Appendix*, Fig. S3).

The nonlinear trend of f_{org} as a function of sea level is paralleled by the calculated burial flux of organic carbon, where a sweet spot optimum occurs at intermediate sea levels (Fig. 4*B*, see *SI Appendix*). One interpretation of this sweet spot optimum is that the low sea level side of the optimum is associated with a slow-down in weathering supply of P_{aq} during cooling and ice-sheet growth under colder climatic conditions. Such a weathering reduction would have caused a decrease in P_{aq}, diverting the runaway P_{aq}-rich and anoxic ocean predicted by Bjerrum's model with a nondynamic P influx from continents (7) (Figs. 1*A* and 5). By contrast, the observed continuous benthic foraminifera record suggests that the deep ocean remained oxic during the Cenozoic.

Alternatively, P_{aq} may have been reduced at low sea levels due to vertical migration of the OMZs relative to P_{reac} rich shelf sediments. For phosphate to be remobilized by OMZs and catalyze extended periods of ocean productivity, then the OMZs must impinge on P_{reac} rich sediments, predominantly on the continental

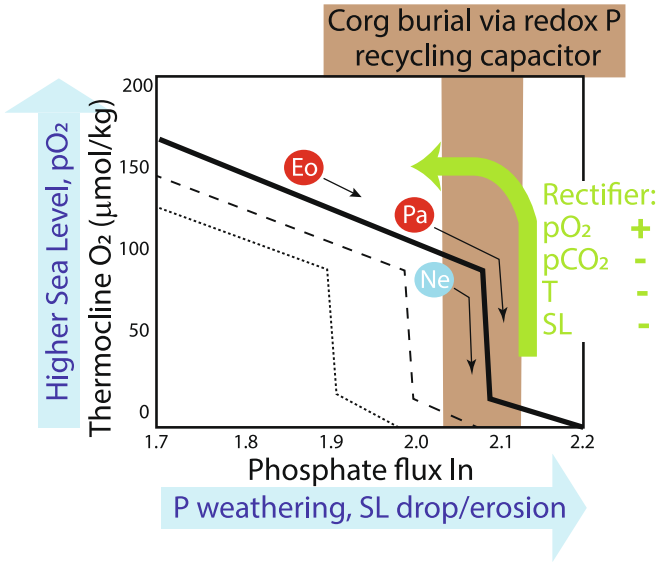

Fig. 5. Schematic adapted from the transient model simulations of (*SI Appendix*, figure S12*B* from ref. 7) to show the minimum water-column oxygen concentration vs. the input phosphate whereby thermocline waters close to a critical oxygen concentration (~90 µmol/kg), with a small additional input of P (black arrows), can lead to a threshold behavior in C_{org} burial. This critical oxygen concentration is sensitive to the weathering inputs of phosphate, which dictate the oxygen demand of organic matter produced; or to the temperature dependence of the solubility of oxygen in the water column, or to the atmospheric oxygen content. As such the relationship between the O_2 threshold and sea level is not absolute but varies, dependent on these drivers of the background seawater chemistry. Small P increases to the ocean from erosion or residence time changes associated with sea-level rise or fall can be amplified through the redox release of P from coastal sediments and lead to a significant increase in organic carbon burial. Also plotted in the red and blue circles is the approximate position of the climate system before the sea-level rise events identified in Fig. 3 with respect to the threshold, with arrows indicating the perturbation by a small P input. For short-term perturbations, the system naturally rectifies by burying sufficient carbon to either decrease sea level and move the OMZs off the continental shelf, or decreasing temperature which raises the O_2 content of the water column. On longer timescales, the build-up of O_2 from the burial of C_{org}, raises the O_2 content of the water column and rectifies the system. Also shown, in gray, are hypothetical curves of how the threshold may move with lower atmospheric O_2 content, or much warmer water columns with lower O_2 concentrations due to solubility. Although this schematic suggests that the ocean tends to anoxia in the OMZs with even greater P input, as discussed and shown in Fig. 1, it is likely that the deepening of the OMZs beyond the continental shelf, as revealed by the data here, represents a lower threshold to the behavior.

shelf, yielding the highest rate of redox-dependent release of phosphate from those organic-rich sediments (Fig. 1). With greater sea-level recession, the OMZs may drop deeper than the depths of the P_{reac}-rich sediments of the continental shelf. This is the situation in the modern ocean, where the OMZs are deeper than the continental shelf (75) and associated with low sedimentation rates (11), limiting the potential P regeneration. In our record, the optimum for the OMZ to coincide with C_{org}-rich continental shelf sediments and propagate C_{org} burial appears to be close to ~+10 to +40 m above modern sea level (Fig. 2). At such intermediate sea levels, the top of the OMZ [at present at ~−100 to −150 m (76)], would impinge fully on the modern continental shelf (−120 m to 0 m at present), allowing a maximum of C_{org} burial. In addition, colder ocean conditions associated with low sea level would further have deepened the OMZs through the temperature dependence of remineralization rates (77, 78).

Carbon Cycle Feedbacks. Sea-level control on P_{aq} acts together with a sedimentation rate and redox-sensitive C_{org}/P_{reac} to change the gearing of C_{org} burial per mole of P supplied from weathering to create a sweet spot of high C burial rates at intermediate sea levels (16, 79 and Fig. 4*B*). The total burial of organic carbon can change with sea level even though the input and burial of P_{reac} may remain unchanged (7).

Near the O_2 threshold, the redox-dependent acceleration of C_{org} burial acts as a fast positive-feedback (4, 80), hastening the onset of glaciation, or as a dynamic rectifier. Any perturbation to higher sea levels leads to extensive C_{org} burial, which drives the climate back to a cooler state. For example, the inundated continental shelf of interglacial periods yields higher C_{org} burial rates, more positive $\delta^{13}C$ (81), and a natural oscillation back to a lower CO_2 glaciation (20, 82, 83). Over the Cenozoic, the maximum change in the proportional C_{org} flux, from 0.21 to 0.35, represents only an approximate 20% increase in the *total* C sink. The C burial events persist for <5 My (Fig. 3) and are small enough and insufficiently long-lived to drive an imbalance with weathering supply and toward a runaway icehouse (84). But the C burial events may be sufficiently dynamic to maintain a resilient icehouse against smaller warming perturbations, demanding a driver to a sea level higher than +40 m, to return to persistent greenhouse conditions (Fig. 4*A*).

The intermediate shelf-area sweet spot for high organic C burial rates is inherently self-limiting due to the drawdown in atmospheric CO_2. Associated cooling and ice-sheet growth deepens the OMZs through decreased temperature or sea level, sliding the OMZs off the continental shelf and deeper than the optimal P_{reac} release, thus reducing C_{org} burial (Fig. 1*C*). Alternatively, redox-driven P_{reac} release may be limited by a slower negative-feedback due to elevated atmospheric oxygen from high organic carbon burial that reoxygenates the ocean (2, 9) invoked to generate self-sustaining oscillations (79). This oscillation may apply to the Cenozoic cycles in proportional organic C burial, with an approximate wavelength of ~5 My, after the Eocene period of P_{aq} starvation.

Implications for the Total Sedimentary Carbon Sink. Given the link between P_{aq} limitation of the C_{org} flux to sediments and high CO_2 in the atmosphere during the Eocene (56 to 33.9 Ma), a deceleration in the sedimentary carbon sink may have contributed to an accumulation of ocean-atmosphere CO_2. A more detailed C_{org} flux calculation, accounting for shelf (85–87) and pelagic $CaCO_3$ accumulation (88, 89), suggests that, to a first order, the Eocene experienced limited carbon burial (*SI Appendix*, *SI Text* and Fig. 6). This reduced carbon sink was terminated by an uptick in shelf C flux starting at ~43 Ma, coincident with a rise in the $^{87}Sr/^{86}Sr$ isotope ratio (69, 70). P_{aq} starvation of the ocean was increasingly alleviated from ~35 Ma onward, promoting a higher total sedimentary flux of both C_{org} and $CaCO_3$ (Fig. 6 and *SI Appendix*, *SI Text*). Pelagic carbonate appears responsive to excess carbon and alkalinity from shelf loss (88, 89) and P_{aq} availability, such that the decline in tropical shelf accumulation (85–87) through the Paleogene is compensated approximately by a similar magnitude increase in the pelagic C flux through the Neogene but with additional sedimentary C pulses when water column P was higher (Fig. 6). Sea level represents a carbon-cycle-feedback via its influence on the redox-dependent availability of P_{aq}, to increase the carbon sink and act as a positive-feedback toward ice-sheet inception, but reduces carbon sinks when ice sheets are larger.

Geological Implications. The sweet spot that allows enhanced organic carbon burial for multimillions of years through redox recycling of P requires a rather unique set of geological ingredients: sufficient P weathering, poising the ocean near the O_2 threshold at 90 µmol/kg in the water column, and a depth of the O_2 minimum that impinges on plentiful organic-rich

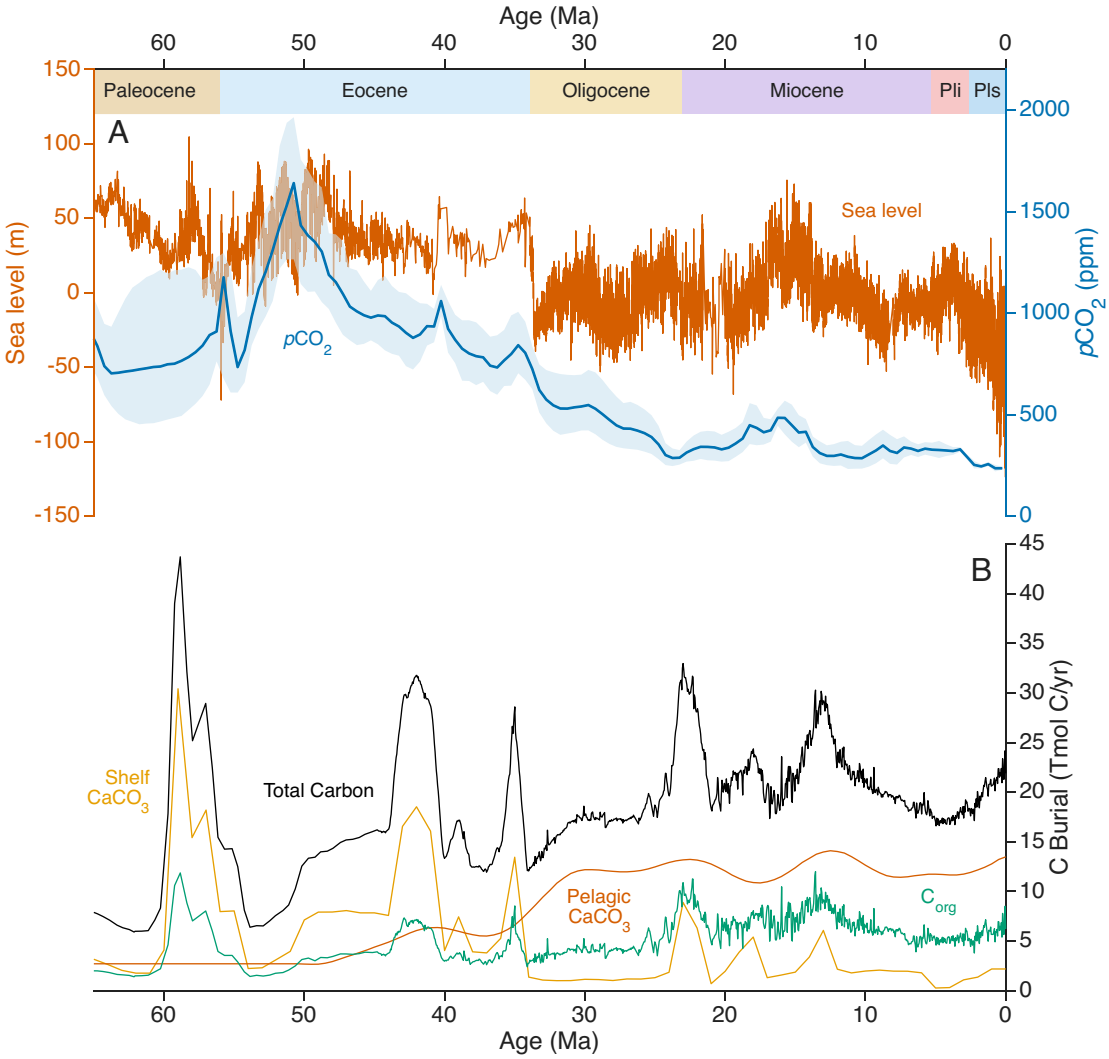

Fig. 6. (*A*) Cenozoic-sea level from Miller et al. (55) and atmospheric pCO_2 from CenCO2PIP (32). (*B*) Total Cenozoic C burial (black, *SI Appendix, SI Text*), reconstructed from the sum of shelf carbonate burial (yellow, 87) and pelagic carbonate burial (orange, 90) divided by (1 - f_{org}). C_{org} burial (green) was reconstructed from total C burial multiplied by f_{org}.

sediments on an extensive continental shelf (Fig. 5). Significant low-latitude continental land mass, tectonism (91), or life on land to accelerate P_{aq} input (92), and a biological pump dominated by eukaryotes (93, 94), yielding an OMZ, may be prerequisites for significant atmospheric O_2 build up, inevitably accompanied by significant glaciation. For any given sea level and phosphate supply, in a past lower pO_2, shallow OMZs would have impinged at shallower depths of the high sedimentation-rate continental shelf, typically containing a higher fraction of C_{org} and P_{reac} for redox recycling. Consequently, the ocean would have been more closely poised to the threshold to allow extensive C_{org} burial for small changes in sea level or perturbations to the P budget (95, 96). With shallower OMZs, there was a much greater areal extent of the continental shelves for persistent phosphate release during sea-level retreat, allowing greater redox recycling of P for longer, before inhibition of the organic carbon burial cycle by build-up of atmospheric oxygen. Such a mechanism speaks to the pulsed nature of O_2 build-up and would have resulted in much higher amplitude glaciations, possibly contributing to the potential for Snowball Earth (97). Glaciations have become more muted as O_2 has accumulated in the atmosphere and since the deepening of the OMZs across the Mesozoic boundary (98) due to the rise of the mineralized plankton. The sweet spot for organic carbon burial has narrowed over time, increasingly stabilizing the climate and atmosphere (96).

Conclusions

Records of f_{org} are consistent with a persistent positive-feedback on the size of the carbon sink where ocean oxygen levels decrease as the Earth became more glaciated during the Cenozoic. The Eocene-ocean (56 to 33.9 Ma) was well oxidized and starved of P_{aq} by the degree of continental shelf inundation, effectively trapping the P with highly efficient shallow C_{org} burial. With progressive glaciation and declining sea levels, the reduced area of continental shelf inundation resulted in P_{aq} increasing in availability, elevating the oxygen demand of the water column until the OMZs emerged in the aftermath of the Eocene/Oligocene boundary (~30 Ma). The presence of subsurface waters with an O_2 content less than 90 μmol/kg that impinge on the C_{org} and P_{reac} rich sediments of the continental shelf represents a rapid-feedback on carbon burial. At sea-level perturbations ~+10 to +40 m above modern, C_{org} burial persists for timescales >1 My due to the redox recycling of phosphate; a scenario which is likely self-limiting. The presented records demonstrate that pulsed burial of organic carbon is likely a persistent feature and rectifier of glaciated worlds.

At lower sea levels still, less than +10 m, the sediment release of P is more limited when the OMZs are deeper than the continental shelf break. As a result, the modern ocean reflects a more anoxic water column than that experienced in the Eocene and likely through the Mesozoic, which counterintuitively harbored the most oxygenated waters, coincident with the warmest periods and highest sea levels. The deepening of the OMZs through time, has been a key factor in stabilizing the climate of the Earth system.

Materials and Methods

I/Ca Analysis. ODP Sites are located on the Walvis Ridge with ODP Site 1262 from 27° 11.15′ S 1°34.62′ E, 4,755 m water depth, and ODP Site 1264 from 28° 31.95′S 2° 50.73′ E and 2,505 m water depth. 3 to 5 mg of coarse-fraction material (> 63 μm) for each sample was weighed, crushed, and rinsed with deionized water to remove residual porewater before dissolution. A previous study (99) showed that the coarse-fraction, without further cleaning by oxidative or reductive reagents, was sufficient to capture the same trend in I/Ca as cleaned, single-genus planktic foraminiferal measurements. I/Ca was measured on a quadrupole inductively coupled plasma mass spectrometer (Bruker M90) at Syracuse University. Carbonate samples were dissolved in 3% nitric acid and diluted to form solutions with ~50 ppm Ca for analyses. Fresh calibration standards, matching the sample matrix, were prepared for every batch of samples. The precision of ^{127}I is typically better than 1% and is not reported separately for each sample. The long-term accuracy is guaranteed by frequent repeats of the reference material JCp-1. The detection limit of I/Ca is typically below 0.1 μmol/mol.

Data, Materials, and Software Availability. Study data are included in the article and/or supporting information.

ACKNOWLEDGMENTS. The project received funding from the European Research Council (ERC) under the European Union's Horizon 2020 research and innovation program (SCOOBI project, grant agreement no. 101019146; REMR) and from the Natural Environment Research Council (NERC; PUCCA project, award NE/V011049/1; REMR). Z.L. is supported by NSF EAR 2323366 and EAR 2121445. C.J.B. is supported by DFF 10.46540/2032-00265B. This research used samples provided by the International Ocean Discovery Program to whom we are grateful. We are endebted to one anonymous reviewer and Thomas Algeo whose comments greatly improved the manuscript.

Author affiliations: [a]Department of Earth Sciences, University of Oxford, Oxford OX1 3AN, United Kingdom; [b]Department of Earth and Environmental Sciences, Syracuse University, Syracuse, NY 13244; and [c]Department of Geosciences and Natural Resource Management, University of Copenhagen, Copenhagen K DK-1350, Denmark

1. J. C. G. Walker, P. B. Hays, J. F. Kasting, A negative feedback mechanism for the long-term stabilization of Earth's surface temperature. *J. Geophys. Res. Oceans* **86**, 9776–9782 (1981), 10.1029/JC086iC10p09776.
2. P. Van Capellan, E. D. Ingall, Redox stabilization of the atmosphere and oceans by phosphorus-limited marine productivity. *Science* **271**, 493–496 (1996).
3. Z. Lu, R. E. M. Rickaby, J. L. Payne, A. N. Prow, Phanerozoic co-evolution of O2-CO2 and ocean habitability. *Natl. Sci. Rev.* **11**, nwae099 (2024).
4. D. Hülse, A. Ridgwell, Instability in the geological regulation of Earth's climate. *Science* **389**, eadh7730 (2025), 10.1126/science.adh7730.
5. R. E. Hecky, P. Kilham, Nutrient limitation of phytoplankton in freshwater environments: A review of recent evidence on the effects of enrichment. *Limnol. Oceanogr.* **33**, 796–822 (1988).
6. C. R. Benitez-Nelson, The biogeochemical cycling of phosphorus in marine systems. *Earth Sci. Rev.* **51**, 109–135 (2000).
7. C. J. Bjerrum, J. Bendtsen, J. J. F. Legarth, Modelling organic carbon burial during sea-level rises with application to the Cretaceous. *Geochem. Geophys. Geosys.* **7**, 1–24 (2006).
8. E. Ingall, R. Jahnke, Evidence for enhanced phosphorus regeneration from marine sediments overlain by oxygen depleted waters. *Geochim. Cosmochim. Acta* **58**, 2571–2575 (1994).
9. P. Van Cappellen, E. D. Ingall, Benthic phosphorus regeneration, net primary production, and ocean anoxia: A model of the coupled marine biogeochemical cycles of carbon and phosphorus. *Paleoceanogr. Paleoclimatol.* **9**, 677–692 (1996).
10. A. S. Colman, H. D. Holland, "The global diagenetic flux of phosphorus from marine sediments to the oceans: Redox sensitivity and the control of atmospheric oxygen levels" in *Marine Authigenesis: From Global to Microbial*, C. R. Glenn, L. Prévôt-Lucas, J. Lucas, Eds. (SEPM Special Publication, 2000), vol. 66, pp. 53–75.
11. D. E. Canfield, C. J. Bjerrum, S. Zhang, H. Wang, X. Wang, The modern phosphorus cycle informs interpretations of Mesoproterozoic Era phosphorus dynamics. *Earth Sci. Rev.* **208**, 103267 (2020).
12. T. J. Algeo, E. Ingall, Sedimentary Corg: P ratios, paleocean ventilation, and Phanerozoic atmospheric pO2. *Palaeogeogr. Palaeoclimatol. Palaeoecol.* **256**, 130–155 (2007).
13. E. D. Ingall, R. M. Bustin, P. Van Cappellen, Influence of water column anoxia on the burial and preservation of carbon and phosphorus in marine shales. *Geochim. Cosmochim. Acta* **57**, 303–316 (1993).
14. E. D. Ingall, P. van Capellan, Relation between sedimentation rate and burial of organic phosphorus and organic carbon in marine sediments. *Geochem. Cosmochim. Acta* **54**, 373–386 (1990).
15. L. D. Anderson, M. L. Delaney, K. L. Faul, Carbon to phosphorus ratios in sediments: Implications for nutrient cycling. *Global Biogeochem. Cycles* **15**, 65–79 (2001), 10.1029/2000GB001270.
16. K. C. Ruttenberg, "The global phosphorus cycle" in *Treatise on Geochemistry*, H. D. Holland, K. K. Turekian, Eds. (Elsevier, New York, 2003), vol. 8, pp. 585–643.
17. K. Wallmann, Feedbacks between oceanic redox states and marine productivity: A model perspective focused on benthic phosphorus cycling. *Glob. Biogeochem. Cycles* **17**, 1084 (2003), 10.1029/2002GB001968.
18. W. H. Berger, Increase of carbon dioxide in the atmosphere during deglaciation: The coral reef hypothesis. *Naturwissenschaften* **69**, 87–88 (1982).
19. B. N. Opdyke, J. C. G. Walker, Return of the coral reef hypothesis: Basin to shelf partitioning of $CaCO_3$ and its effect on atmospheric CO_2. *Geology* **20**, 733–736 (1992).
20. W. S. Broecker, Glacial to interglacial changes in ocean chemistry. *Prog. Oceanogr.* **11**, 151–197 (1982).
21. K. Wallmann, B. Schneider, M. Sarnthein, Effects of eustatic sea-level change, ocean dynamics, and nutrient utilization on atmospheric pCO2 and seawater composition over the last 130 000 years: A model study. *Clim. Past* 12, 339–375 (2016), 10.5194/cp-12-339-2016.
22. O. Cartapanis, D. Bianchi, S. L. Jaccard, E. D. Galbraith, Global pulses of organic carbon burial in deep-sea sediments during glacial maxima. *Nat. Commun.* **7**, 10796 (2016), 10.1038/ncomms10796.
23. O. Cartapanis, E. D. Galbraith, D. Bianchi, S. L. Jaccard, Carbon burial in deep-sea sediment and implications for oceanic inventories of carbon and alkalinity over the last glacial cycle. *Clim. Past* **14**, 1819–1850 (2018).
24. J. M. Hayes, J. R. Waldbauer, The carbon cycle and associated redox processes through time. *Philos. Trans. R. Soc. B Biol. Sci.* **361**, 931–950 (2006).
25. K. H. Freeman, J. M. Hayes, Fractionation of carbon isotopes by phytoplankton and estimates of ancient CO2 levels. *Glob. Biogeochem. Cycles* **6**, 185–198 (1992), 10.1029/92GB00190.
26. S. Poudel *et al.*, Biophysical analysis of the evolution of substrate specificity in RuBisCO. *Proc. Natl. Acad. Sci. U.S.A.* **48**, 30451–30457 (2020).
27. J. M. Hayes, H. Strauss, A. J. Kaufman, The abundance of ^{13}C in marine organic matter and isotopic fractionation in the global biogeochemical cycle of carbon during the past 800 Ma. *Chem. Geol.* **161**, 103–125 (1999).
28. L. A. Derry, Closing the geologic carbon cycle. *Proc. Natl. Acad. Sci. U.S.A.* **121**, e2409333121 (2024).
29. E. Mason, M. Edmonds, S. Turchyn, Remobilization of crustal carbon may dominate volcanic arc emissions. *Science* **357**, 290–294 (2017), 10.1126/science.aan5049.
30. D. H. Rothman, J. M. Hayes, R. E. Summons, Dynamics of the Neoproterozoic carbon cycle. *Proc. Natl. Acad. Sci. U.S.A.* **100**, 8124–8129 (2004).
31. A. J. Boller, P. J. Thomas, C. M. Cavanaugh, K. M. Scott, Low stable carbon isotope fractionation by coccolithophore RubisCO. *Geochim. Cosmochim. Acta* **75**, 7200–7207 (2011).
32. B. Hönisch *et al.*; Cenozoic CO2 Proxy Integration Project (CenCO2PIP) Consortium, Toward a Cenozoic history of atmospheric CO_2. *Science* **382**, eadi5177 (2023), 10.1126/science.adi5177.
33. E. B. Wilkes, R. B. Y. Lee, H. L. O. McClelland, R. E. M. Rickaby, A. Pearson, Carbon isotope ratios of coccolith–associated polysaccharides of Emiliania huxleyi as a function of growth rate and CO_2 concentration. *Org. Geochem.* **119**, 1–10 (2018).
34. T. Westerhold *et al.*, An astronomically dated record of Earth's climate and its predictability over the last 66 million years. *Science* **369**, 1383–1387 (2020).
35. C. R. Witkowski *et al.*, Molecular fossils from phytoplankton reveal secular P_{co2} trend over the Phanerozoic. *Sci. Adv.* **4**, eaat4556 (2018), 10.1126/sciadv.aat4556.
36. N. Chauhan, R. E. M. Rickaby, Size-dependent dynamics of the internal carbon pool drive isotopic vital effects in calcifying phytoplankton. *Geochim. Cosmochim. Acta* **373**, 35–51 (2024).
37. S. Herrmann, H. R. Thierstein, Cenozoic coccolith size changes–Evolutionary and/or ecological controls? *Palaeogeogr. Palaeoclimatol. Palaeoecol.* **333–334**, 92–106 (2012), 10.1016/j.palaeo.2012.03.011.
38. B. Suchéras-Marx, J. Henderiks, Downsizing the pelagic carbonate factory: Impacts of calcareous nannoplankton evolution on carbonate burial over the past 17 million years. *Glob. Planet. Change* **123**, 97–109 (2014), 10.1016/j.gloplacha.2014.10.015.
39. J. N. Young, R. E. M. Rickaby, M. Kapralov, D. Filatov, Adaptive signals in algal Rubisco reveal a history of ancient atmospheric CO_2. *Phil. Trans. Roy. Soc.* **367**, 483–492 (2012).
40. G. G. B. Tcherkez, G. D. Farquhar, T. J. Andrews, Despite slow catalysis and confused substrate specificity, all ribulouse bisphosphate carboxylases may be nearly perfectly optimised. *Proc. Natl. Acad. Sci. U.S.A.* **103**, 7246–7251 (2006).
41. L. R. Kump, M. A. Arthur, "Global chemical erosion during the Cenozoic: Weatherability balances the budget" in *Tectonic Uplift and Climate Change*, W. Ruddiman, Ed. (Plenum, New York, 1997), pp. 399–426, 10.1007/978-1-4615-5935-1.
42. C. Bolton, H. Stoll, Late Miocene threshold response of marine algae to carbon dioxide limitation. *Nature* **500**, 558–562 (2013), 10.1038/nature12448.
43. L. M. Claxton, H. L. O. McClelland, M. Hermoso, R. E. M. Rickaby, Eocene emergence of highly calcifying coccolithophores despite declining atmospheric CO_2. *Nat. Geosci.* **15**, 826–831 (2022).
44. L. Diester-Haass, K. Billups, K. C. Emeis, In search of the late Miocene–early Pliocene "biogenic bloom" in the Atlantic Ocean (Ocean Drilling Program Sites 982, 925, and 1088). *Paleoceanography* **20**, 20 (2005), 10.1029/2005PA001139.
45. M. E. Gastaldello *et al.*, The Late Miocene-Early Pliocene biogenic bloom: An integrated study in the Tasman Sea. *Paleoceanogr. Paleoclimatol.* **38**, e2022PA004565 (2023), 10.1029/2022pa004565.
46. B.T. Karatsolis, B. C. Lougheed, D. D. Vleeschouwer, J. Henderiks, Abrupt conclusion of the late Miocene-early Pliocene biogenic bloom at 4.6-4.4 Ma. *Nat. Commun.* **13**, 353 (2022), 10.1038/s41467-021-27784-6.
47. E. S. C. Anttila *et al.*, Timing and tempo of organic carbon burial in the Monterey Formation of the Santa Barbara Basin and relationships with Miocene climate. *Earth Planet. Sci. Lett.* **620**, 118343 (2023), 10.1016/j.epsl.2023.118343.

48. L. A. Derry, C. France-Lanord, Neogene growth of the sedimentary organic carbon reservoir. *Paleoceanography* **11**, 267–275 (1996), 10.1029/95PA03839.
49. K. Kurtz, L. R. Kump, M. A. Arthur, J. C. Zachos, A. Paytan, Early Cenozoic decoupling of the global carbon and sulfur cycles. *Paleoceanography* **18**, 1–14 (2003), 10.1029/2003pa000908.
50. N. Komar, R. E. Zeebe, G. R. Dickens, Understanding long-term carbon cycle trends: Late Paleocene through the early Eocene. *Paleoceanogr. Paleoclimatol.* **28**, 650–662 (2013), 10.1002/palo.20060.
51. L. Diester-Haass, K. Billups, K. Emeis, Enhanced paleoproductivity across the Oligocene/Miocene Boundary as evidenced by benthic foraminiferal accumulation rates. *Paleogeogr. Paleoclimatol. Paleoecol.* **302**, 464–473 (2011).
52. H. D. Klemme, G. F. Ulmishek, Effective petroleum source rocks of the world: Stratigraphic distribution and controlling depositional factors. *Bull. Am. Assoc. Petrol. Geol.* **75**, 1809–1851 (1991).
53. J. B. Smaers *et al.*, The evolution of mammalian brain size. *Sci. Adv.* **7**, eabe2101 (2021), 10.1126/sciadv.abe2101.
54. R. E. M. Rickaby, T. J. Wood, R. Gollnisch, C. Bjerrum, Z. Lu, Indicators and evolutionary consequences of the Cenozoic history of Oxygen. *Cold Spring Harb. Perspect. Biol.* (2026), 10.1101/cshperspect.a041923 (accepted).
55. K. G. Miller *et al.*, Cenozoic sea-level and cryospheric evolution from deep-sea geochemical and continental margin records. *Sci. Adv.* **6**, eaaz1346 (2020), 10.1126/sciadv.aaz1346.
56. K. B. Follmi, The phosphorus cycle, phosphogenesis and marine phosphate-rich deposits. *Earth Sci. Rev.* **40**, 55–124 (1996).
57. A. Olivarez Lyle, M. W. Lyle, Missing organic carbon in Eocene marine sediments: Is metabolism the biological feedback that maintains end-member climates. *Paleoceanogr. Paleoclim.* **21**, PA2007 (2006). 10.1029/2005PA001230.
58. Z. Li, Y. G. Zhang, M. Torres, B. J. W. Mills, Neogene burial of organic carbon in the global ocean. *Nature* **613**, 90–95 (2023), 10.1038/s41586-022-05413-6.
59. C. J. Bjerrum, J. Bendtsen, Relations between long term sea-level change, shelf-ocean exchange and shelf burial of organic material. *Eos Trans. AGU* **83**, Ocean Sci. Meet.Suppl., Abstract OS41G-08 (2002).
60. J. D. Asanbe, J. Henderiks, Major shifts in Equatorial Atlantic and Pacific calcareous Nannofossil assemblages across the Early Eocene Climatic Optimum (EECO; 53–49 Ma). *Paleoceanogr. Paleoclimatol.* **40**, e2024PA005038 (2025), 10.1029/2024PA005038.
61. R. M. Leckie, T. J. Bralower, R. Cashman, Oceanic Anoxic events and plankton evolution: Biotic response to tectonic forcing during the mid-Cretaceous. *Paleoceanogr. Paleoclim.* **17**, e2001PA000623 (2002), 10.1029/2001PA000623.
62. S. Tozzi, O. Schofield, P. Falkowski, Historical climate change and ocean turbulence as selective agents for two key phytoplankton functional groups. *Mar. Ecol. Prog. Ser.* **274**, 123–132 (2004).
63. C. P. Slomp, J. Thompson, G. De Lange, Enhanced regeneration of phosphorus during formation of the most recent Eastern Mediterranean sapropel (S1). *Geochim. Cosmochim. Acta* **66**, 1171–1184 (2002).
64. X. Wang, R. E. M. Rickaby, Z. Lu, A deep dive into the planktic foraminiferal I/Ca in global core-tops. *Glob. Planet. Change* **261**, 105412 (2026).
65. Z. Lu, H. C. Jenkyns, R. E. M. Rickaby, I/Ca ratios in marine carbonate as a palaeo-redox proxy during oceanic anoxic events. *Geology* **38**, 1107–1110 (2010).
66. Z. Lu *et al.*, Oxygen depletion recorded in upper waters of the glacial Southern Ocean. *Nat. Commun.* **7**, 11146 (2016), 10.1038/ncomms11146.
67. W. Lu *et al.*, Refining the planktic foraminiferal I/Ca proxy: Results from the Southeast Atlantic Ocean. *Geochim. Cosmochim. Acta* **287**, 318–327 (2020).
68. A. Auderset *et al.*, Enhanced ocean oxygenation during Cenozoic warm periods. *Nature* **609**, 77–82 (2022).
69. J. K. Caves, A. B. Jost, K. V. Lau, K. Maher, Cenozoic carbon cycle imbalances and a variable weathering feedback. *Earth Planet. Sci. Lett.* **450**, 152–163 (2016), 10.1016/j.epsl.2016.06.035.
70. J. Veizer *et al.*, 87Sr/86Sr, δ13C and δ18O evolution of Phanerozoic seawater. *Chem. Geol.* **161**, 59–88 (1999).
71. K. Kayano, Y. Shiraiwa, Physiological regulation of coccolith polysaccharide production by phosphate availability in the coccolithophorid Emiliania huxleyi. *Plant Cell Physiol.* **50**, 1522–1531 (2009), 10.1093/pcp/pcp097.
72. S. Gill, Q. Zhang, G. M. Henderson, R. E. M. Rickaby, The physiological response of contrasting coccolithophore species to Ocean Alkalinity Enhancement. *J. Geophys. Res. Biogeosci.* **130**, e2025JG009103 (2025), 10.1029/2025JG009103.
73. K. Billups, R. E. M. Rickaby, D. P. Schrag, Cenozoic pelagic Sr/Ca records: Exploring a link to paleoproductivity. *Paleoceanography* **19**, PA3005 (2004).
74. Z. V. Finkel, M. E. Katz, J. D. Wright, O. M. Schofield, P. G. Falkowski, Climatically driven macroevolutionary patterns in the size of marine diatoms over the Cenozoic. *Proc. Natl. Acad. Sci. U.S.A.* **102**, 8927–8932 (2005), 10.1073/pnas.0409907102.
75. J. Karstensen, L. Stramma, M. Visbeck, Oxygen mimumum zones in the eastern tropical Atlantic and Pacific oceans. *Progr. Oceanogr.* **77**, 331–350 (2008).
76. A. Paulmier, D. Ruiz-Pino, Oxygen minimum zones (OMZs) in the modern ocean. *Prog. Oceanogr.* **80**, 113–128 (2009).
77. C. M. Marsay *et al.*, Attenuation of sinking particulate organic carbon flux through the mesopelagic ocean. *Proc. Natl. Acad. Sci. U.S.A.* **112**, 1089–1094 (2015), 10.1073/pnas.1415311112.
78. E. Y. Kwon, F. Primeau, J. L. Sarmiento, The impact of remineralization depth on the air-sea carbon balance. *Nat. Geosci.* **2**, 630–635 (2009), 10.1038/ngeo612.
79. I. C. Handoh, T. M. Lenton, Periodic mid-Cretaceous oceanic anoxic events linked by oscillations of the phosphorus and oxygen biogeochemical cycles. *Global Biogeochem. Cycles* **17**, 1092 (2003), 10.1029/2003GB002039.
80. C. J. Bjerrum, Sea level, climate, and ocean poisoning by sulfide all implicated in the first animal mass extinction. *Geology* **46**, 575–576 (2018).
81. K. I. C. Oliver *et al.*, A synthesis of marine sediment core $\delta^{13}C$ data over the last 150 000 years. *Clim. Past* **6**, 645–673 (2010).
82. M. Adloff, A. Jeltsch-Thommes, F. Poppelmeier, T. F. Stocker, F. Joos, Sediment fluxes dominate glacial–interglacial changes in ocean carbon inventory: Results from factorial simulations over the past 780000 years. *Clim. Past* **21**, 571–592 (2025), 10.5194/cp-21-571–2025.
83. A. C. Fowler, R. E. M. Rickaby, E. Wolff, Exploration of a simple model for ice ages. *GEM - Int. J. Geomathematics* **4**, 227–297 (2012), 10.1007/s13137-012-0040-7.
84. Y. Godderis, Y. Donnadieu, B. J. W. Mills, What models tell us about the evolution of carbon sources and sinks over the Phanerozoic. *Annu. Rev. Earth Planet. Sci.* **51**, 471–492 (2023), 10.1146/annurev-earth-032320-092701.
85. B. N. Opdyke, B. H. Wilkinson, Surface area control of shallow cratonic to deep marine carbonate accumulation. *Paleoceanography* **3**, 685–703 (1988), 10.1029/PA003i006p00685.
86. T. Salles *et al.*, Carbonate burial regimes, the Meso-Cenozoic climate, and nannoplankton expansion.. *Proc. Natl. Acad. Sci. U.S.A.* **122**, e2516468122 (2025), 10.1073/pnas.2516468122.
87. J. M. Husson, S. E. Peters, Shifting carbonate burial between oceanic and continental crust across Earth history. *Earth Planet. Sci. Lett.* **677**, 119810 (2026), 10.1016/j.epsl.2025.119810.
88. G. J. A. Brummer, A. J. M. Eijden, "Blue-ocean" paleoproductivity from pelagic carbonate mass accumulation rates. *Mar. Micropal.* **19**, 99–117 (1992).
89. A. Dutkiewicz, R. D. Müller, The history of Cenozoic carbonate flux in the Atlantic Ocean constrained by multiple regional carbonate compensation depth reconstructions. *Geochem. Gephys. Geosys.* **23**, e2022GC010667 (2002), 10.1029/2022GC010667.
90. B. P. Boudreau, Y. Luo, Retrodiction of secular variations in deep-sea CaCO3 burial during the Cenozoic. *Earth Planet. Sci. Lett.* **474**, 1–12 (2017), 10.1016/j.epsl.2017.06.005.
91. C. R. Walton *et al.*, Evolution of the crustal phosphorus reservoir. *Sci. Adv.* **9**, eade6923 (2023), 10.1126/sciadv.ade6923.
92. B. Peret *et al.*, Root architecture responses: In search of phosphate. *Plant Physiol.* **166**, 1713–1723 (2014).
93. N. J. Butterfield, Oxygen, animals and aquatic bioturbation: An updated account. *Geobiology* **16**, 3–16 (2018), 10.17863/CAM.21972.
94. T. M. Lenton, R. A. Boyle, S. W. Poulton, G. A. Shields-Zhou, N. J. Butterfield, Co-evolution of eukaryotes and ocean oxygenation in the Neoproterozoic Era. *Nat. Geosci.* **7**, 257–265 (2014).
95. M. S. Dodd *et al.*, Marine phosphorus and atmospheric oxygen were coupled during the Great Oxidation Event. *Nat. Commun.* **16**, 9151 (2025), 10.1038/s41467-025-64194-4.
96. A. Bachan *et al.*, A model for the decrease in amplitude of carbon isotope excursions across the Phanerozoic. *Am. J. Sci.* **317**, 641–676 (2017), 10.2475/06.2017.01.
97. P. F. Hoffman, D. P. Schrag, The Snowball Earth hypothesis: Testing the limits of global change. *Terra Nova* **14**, 129–155 (2002).
98. W. Lu *et al.*, Late inception of a persistently oxygenated upper ocean. *Science* **361**, eaar5372 (2018). 10.1126/science.aar5372.
99. X. Zhou, E. Thomas, R. E. M. Rickaby, A. M. E. Winguth, Z. Lu, I/Ca evidence for upper ocean deoxygenation during the Paleocene-Eocene Thermal Maximum (PETM). *Paleoceanography* **29**, 964–975 (2014), 10.1002/2014PA002702.